Monte Carlo study of the low-temperature mobility of electrons in a strained Si layer grown on a $Si_{1-x}Ge_x$ substrate

Toshishige Yamada, H. Miyata,* J.-R. Zhou, and D. K. Ferry
Center for Solid State Electronics Research, Arizona State University, Tempe, Arizona 85287-6206
(Received 9 August 1993)

A Monte Carlo approach is used to study the electron mobility in the $Si/Si_{1-x}Ge_x$ system at low temperatures. The diffusion constant is evaluated in near thermal equilibrium simulations and is converted to the mobility by use of the Einstein relation for a degenerate two-dimensional electron gas. A modulation-doped structure is considered, where the doped $Si_{0.7}Ge_{0.3}$ layer provides channel electrons and is separated from the channel by an undoped $Si_{0.7}Ge_{0.3}$ spacer layer. The electron density is evaluated as a function of spacer width and doping concentration. Electrons are assumed to be only in the lowest subband. Acoustic-phonon scattering and remote impurity scattering determine the possible mobility that can be reached. We find mobility values of 2.5×10^5 cm^2/V s at 4.2 K and 3.1×10^5 cm^2/s at 1.5 K for an electron density of 7.5×10^{11} cm^{-2} (for typical choices of parameters: 10-nm spacer and 2×10^{18} cm^{-3} doping). Peak mobility values of 5.0×10^5 cm^2/V s at 4.2 K and 7.6×10^5 cm^2/s at 1.5 K are possible for wider spacer layer widths, with subsequently lower channel electron densities. The effects of surface roughness scattering, as well as other scatterers are discussed. These processes can be a mechanism to explain the difference between the above ideal mobility and the reported experimental data.

I. INTRODUCTION

There has been significant progress in efforts to achieve high electron mobility in a modulation-doped strained Si layer grown on a relaxed $Si_{1-x}Ge_x$ substrate.[1-4] Experimentally observed mobility values typically are 175 000 cm^2/V s below 4.2 K, 9500 cm^2/V s at 77 K, and 1600 cm^2/V s at 300 K,[1-3] which are well above those of bulk Si, and exhibit a profound potential for device applications. In fact, a high-transconductance n-type $Si/Si_{1-x}Ge_x$ modulation-doped field-effect transistor has been created[4] with 600 mS/mm at 77 K for a gate length of 0.25 μm. In this $Si/Si_{1-x}Ge_x$ system, a two-dimensional (2D) electron gas is created in the strained Si(100) layer, which is grown on a relaxed $Si_{1-x}Ge_x$(100) substrate. Once the heterojunction is formed, the strain at the interface causes the sixfold-degenerate valleys in Si to split into two groups: two lowered valleys that exhibit the longitudinal mass normal to the heterointerface and four raised valleys that have the longitudinal mass parallel to the interface.[5] The conduction band formed by the lowered valleys is now lower than that of $Si_{1-x}Ge_x$ and the band alignment across the heterojunction creates a potential barrier for electrons, so that a type-II superlattice is formed.[5] The electrons prefer to populate the lowered valleys, which are energetically favored, and exhibit the smaller transverse mass in transport phenomena. The energy separation of the valleys effectively reduces the intervalley phonon scattering of the electrons. These two effects result in electron transport properties superior to those of unstrained bulk Si. Previously, we have carried out an ensemble Monte Carlo simulation[6] to study the high-field transport properties of this system at 77 and 300 K, using a three-dimensional (3D) electron model and classical statistics. It was found that the mobility was enhanced significantly, 23 000 cm^2/V s at 77 K and 4000 cm^2/V s at 300 K. The saturation velocity was increased slightly compared with the bulk value at both temperatures. A significant velocity overshoot several times larger than the saturation velocity was also found.

In this paper, we report the results of a Monte Carlo study of the transport properties of this system at low temperatures, where the quantization effect of electron motion normal to the heterointerface and the role of the Fermi statistics are relevant. Because of the Monte Carlo method used, any complicated angular dependence of the various scattering potentials is easily incorporated in the simulation, and the direct use of Mathiessen's rule is avoided. We consider a modulation-doped structure, where the doped $Si_{0.7}Ge_{0.3}$ layer provides channel electrons (the choice $x=0.3$ seems standard[1-3] and is used here) and is separated by an undoped $Si_{0.7}Ge_{0.3}$ spacer layer. Two-dimensional electrons are assumed to reside only in the lowest subband and are described by a Fang-Stern-Howard wave function.[7] The areal electron density is a function of the spacer width and the doping concentration and is calculated by solution of Poisson's equation within the depletion approximation.[8] Acoustic phonon scattering and remote impurity scattering are always present and combine to determine the highest possible mobility. We study this in detail. All other scatterers, such as interface/background impurity scattering or surface roughness scattering, can be made smaller by technological improvements in the crystal and interface quality and are discussed briefly. Screening is included by employing a temperature- and momentum-dependent polarizability function,[9] which is important in explaining the

low-temperature mobility in metal-oxide-semiconductor field-effect-transistors (FET), and also is expected to be important here.[10] The inclusion of the Pauli exclusion principle is essential and this is achieved by using the electron initial energy distribution function in the product $f(E)[1-f(E)]$, where $f(E)$ is a Fermi distribution function at a given temperature. The diffusion constant D is calculated with a standard Monte Carlo technique by evaluation of the mean-square displacement under the influence of appropriate scattering mechanisms and is converted to the mobility μ by use of the Einstein relation for a 2D degenerate electron gas.

We have found that, for a spacer layer of 10 nm and a doping of 2×10^{18} cm^{-3}, the electron density is approximately 7.5×10^{11} cm^{-2} and the largest possible mobility (limited by acoustic phonon and remote impurity scattering) is 2.5×10^{5} cm^2/V s at 4.2 K and 3.1×10^{5} cm^2/V s at 1.5 K. The experimentally observed values, e.g., 175 000 cm^2/V s below 4.2 K by Többen *et al.*, are somewhat smaller than this value and the difference can be attributed to surface roughness scattering and/or interface/background impurity scattering. In Sec. II, the simulation method is explained and the results are discussed in Sec. III. The conclusion is given in Sec. IV.

II. SIMULATION METHOD

In experiments,[1-3] a modulation-doped structure was adopted to achieve high transconductance. In order to find the 2D electron density, n_s as a function of the spacer layer width d, and the doping density N_{SiGe} in the $Si_{0.7}Ge_{0.3}$ layer, we solve a one-dimensional Poisson equation with an appropriate boundary condition.[8] Electrons are assumed to populate only the lowest subband. Since the state density is constant in a 2D system, the 2D electron density n_s is given in closed form as a function of the Fermi energy E_F measured from the bottom of the potential wall, by integration of the Fermi-Dirac function, as[11]

$$n_s=\frac{g_v g_s m_t k_B T}{2\pi\hbar^2}\ln\{1+\exp[(E_F-E_0)/k_B T]\}\ , \quad (1)$$

where g_v and g_s are valley and spin degeneracy factors, respectively (both values are 2 in the present situation of the two lowered valleys). The transverse effective mass m_t (transport mass) in the direction parallel to the interface is used. Here $\hbar$ is the reduced Planck constant, k_B Boltzmann's constant, and T the temperature.

$$E_0=(\hbar^2/2m_l)^{1/3}(3\pi eE_{\mathrm{Si}}/2)^{2/3}(3/4)^{2/3}\ , \quad (2)$$

where the longitudinal effective mass m_l (quantization mass) normal to the interface is used, and E_{Si} is the interface electric field on the Si side. With neglect of the ionized impurities at the interface and in the Si side, we have

$$en_s=\epsilon_{\mathrm{Si}}E_{\mathrm{Si}}=\epsilon_{\mathrm{SiGe}}E_{\mathrm{SiGe}}\ , \quad (3)$$

where e is the unit charge, ϵ_{Si} is the dielectric constant for Si, ϵ_{SiGe} is the dielectric constant for $Si_{0.7}Ge_{0.3}$, and E_{SiGe} is the interface electric field on the $Si_{0.7}Ge_{0.3}$ side. The interface electric field E_{SiGe} can be found by solution of Poisson's equation for the electric potential $V(z)$, with z being the coordinate normal to the interface, and the point $z=0$ corresponds to the interface in Fig. 1 that shows the conduction band alignment. Here $z<0$ corresponds to the sufficiently thick $Si_{0.7}Ge_{0.3}$ region including the spacer and $z>0$ corresponds to the strained Si channel region. Poisson's equation is then given by

$$d^2V/dz^2=-\frac{e}{\epsilon_{\mathrm{SiGe}}}N(z)\ , \quad (4)$$

where $N(z)$ is the ionized impurity donor density in the $Si_{0.7}Ge_{0.3}$ region. Within the depletion approximation, we assume $N(z)=0$ for $-d<z<0$ and $z<-d-w$, and $N(z)=N_{\mathrm{SiGe}}$ for $-d-w<z<-d$, where w is the depletion region thickness of the $Si_{0.7}Ge_{0.3}$ layer and d is the spacer thickness; i.e., we assume no interface and background charges. The boundary condition is such that $V(0)=0$, $dV(0^-)/dz=-E_{\mathrm{SiGe}}$, and $dV(-d-w)/dz=0$. We can solve (4) for $V(-d-w)$, which is given by

$$\epsilon_{\mathrm{SiGe}}E_{\mathrm{SiGe}}=[2eV(-d-w)\epsilon_{\mathrm{SiGe}}N_{\mathrm{SiGe}}+(edN_{\mathrm{SiGe}})^2]^{1/2}-edN_{\mathrm{SiGe}}\ . \quad (5)$$

We assume that $eV(-d-w)=\Delta E_c-E_F$ by consideration of the band structure across the interface, with neglect of the donor level in $Si_{0.7}Ge_{0.3}$, since it is much smaller than ΔE_c. Then, (5) gives E_{SiGe}, which is $en_s/\epsilon_{\mathrm{SiGe}}$ by (3), once the modulation structure is specified with N_{SiGe} and d, and the Fermi energy E_F is known. Practically, we can numerically calculate E_F and n_s as a function of N_{SiGe} and d by the following procedure: Assume a small initial trial E_F, then the 2D electron density n_s is given by (1) with the help of (2), and is converted to E_{SiGe} by (3). This value for E_{SiGe} has to be consistent with (5). If it is not, then E_F is increased until (5) is satisfied. Once E_F and therefore n_s is found, the depleted width w of the doped $Si_{0.7}Ge_{0.3}$ is given by $w=n_s/N_{\mathrm{SiGe}}$, due to the charge neutrality condition.

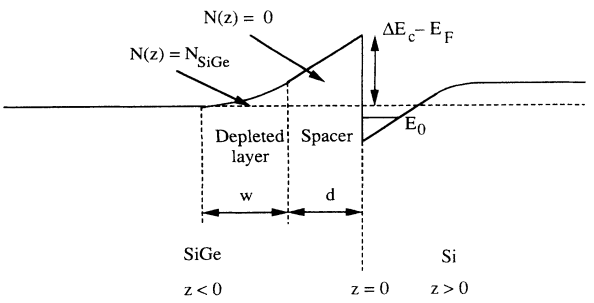

FIG. 1. Conduction-band diagram of the modulation-doped Si/SiGe structure.

Thus w has the same functional dependence as n_s. The results will be illustrated in Sec. III.

Electrons are assumed to reside only in the lowest subband throughout the simulation and their variational envelope function normal to the heterointerface is written by[7,12]

$$\phi(z)=(b_0/2)^{1/2}z\exp(-b_0z/2)\ , \tag{6}$$

where the quantity b_0 indicates the inverse of the quantum well width, given by[7,12]

$$b_0=\left[\frac{33m_le^2n_s}{8\epsilon_{\rm Si}\hbar^2}\right]^{1/3}\ , \tag{7}$$

where the quantization mass m_l is used in (7).

The relevant scattering processes at low temperature arise from remote impurities in the doped $Si_{0.7}Ge_{0.3}$ layer, acoustic phonon scattering, surface roughness scattering at the heterointerface, scattering from impurities at the heterointerface, and scattering from impurities in the strained Si channel layer. The first two processes define the fundamental limit to the mobility, since they cannot be removed by improved technology. The last three (in principle) can be reduced. The heterointerface can be smoothed and purified, and the strained Si channel can also be purified as the technology advances. Therefore, we mainly study the first two processes in order to place a limit on the mobility. We discuss other processes briefly, in connection with the discussion of previously reported experimental data.

As pointed out before,[10] the realistic inclusion of screening is important in the discussion of the low-temperature behavior of the mobility. We have adopted a temperature-momentum-dependent polarizability function Π for the 2D electrons in the lowest subband in the FET structure, which is[9]

$$\Pi(q,T)=\frac{1}{4k_BT}\int_0^\infty \Pi_0(q,\zeta)\cosh^{-2}\left[\frac{(E_F-E_0-\zeta)}{2k_BT}\right]d\zeta\ , \tag{8}$$

where

$$\Pi_0(q,\zeta)=1-\Theta[q-2k(\zeta)]\{1-[2k(\zeta)/q]^2\}^{1/2}\ , \tag{9}$$

$$k(\zeta)=(2m_t\zeta)^{1/2}/\hbar\ , \tag{10}$$

and Θ is the Heavyside function.

The final form of the impurity scattering rate $\Gamma_{\rm imp}$ for an electron with the momentum amplitude k is given by[11,12]

$$\Gamma_{\rm imp}(k)=\frac{e^4}{16\pi^2\epsilon_{\rm SiGe}^2}\frac{g_vg_sm_t}{\hbar^3}\times\int dz\,N_{\rm imp}\int_0^{2\pi}d\theta\,G^2(q,z)q^{-2}\times[1+q_0F(q)\Pi(q)/q]^{-2}\ , \tag{11}$$

where q is the momentum transfer and is related to the electron momentum k by $q=2k\sin\theta/2$ with the scattering angle θ formed by the initial and final momenta of the electron. $N_{\rm imp}$ is the 3D distribution of the impurities and the integration with respect to z is performed over the region where the impurities are located. The degeneracy factors g_v and g_s arise from the density of states. The parameter q_0 in (11) is defined by

$$q_0=\frac{g_vg_sm_t}{2\pi\hbar^2}\frac{e^2}{\epsilon_{\rm SiGe}+\epsilon_{\rm Si}}\ , \tag{12}$$

which is the inverse screening length (modified by $F\times\Pi$) and again the degeneracy factors g_v and g_s are introduced in (12). Note that the transport mass m_t is used in q_0, in contrast to b_0 evaluated with the quantization mass m_l in (7). The factor $G(q,z)^2/[1+q_0F(q)\Pi(q)/q]^{-2}$ in (11) represents the screening effect of the electrons in the lowest subband of the modulation-doped structure. The remote, interface, and background impurity scattering can be treated by this expression in a unified manner. The functions $F(q)$ and $G(q,z)$ take the forms[11,12]

$$F(q)=\frac{1}{16}\left[1+\frac{\epsilon_{\rm SiGe}}{\epsilon_{\rm Si}}\right]\left[8+\frac{9q}{b_0}+\frac{3q^2}{b_0^2}\right]\left[1+\frac{q}{b_0}\right]^{-3}+\frac{1}{2}\left[1-\frac{\epsilon_{\rm SiGe}}{\epsilon_{\rm Si}}\right]\left[1+\frac{q}{b_0}\right]^{-6}\ , \tag{13}$$

$$G(q,z)=\begin{cases}\left[\dfrac{b_0}{b_0+q}\right]^3\exp(qz) & \text{for } z<0\\ \dfrac{1}{2}\left[1+\dfrac{\epsilon_{\rm SiGe}}{\epsilon_{\rm Si}}\right]P(z)+\dfrac{1}{2}\left[1-\dfrac{\epsilon_{\rm SiGe}}{\epsilon_{\rm Si}}\right]\left[\dfrac{b_0}{b_0+q}\right]^3\exp(-qz) & \text{for } z>0\end{cases} \tag{14}$$

where the expression for $z<0$ in (14) is used for remote and interface impurity and the one for $z>0$ is used for background impurity. The function $P(z)$ is defined by[11,12]

$$\begin{aligned}P(z)&=\left[\frac{b_0}{b_0-q}\right]^3[\exp(-qz)-(a_0+a_1z+a_2z^2)\exp(-b_0z)]\ ,\\ a_0&=\frac{2q(3b_0^2+q^2)}{(b_0+q)^3}\ ,\\ a_1&=\frac{4b_0q(b_0-q)}{(b_0+q)^2}\ ,\\ a_2&=\frac{q(b_0-q)^2}{b_0+q}\ ,\end{aligned} \tag{15}$$

where an appropriate limit is taken for the case of $q=b_0$. Both $F(q)$ in (13) and $G(q,z)$ in (14) are the averaged 2D Fourier coefficients (form factor) of the 2D Coulomb potential, but the averages with a weight factor $|\phi(z)|^2$ in the z direction are taken differently in both functions. Writing the 2D Fourier coefficient $V(q,z-z')$ of the Coulomb potential $V(\mathbf{r}-\mathbf{r}',z-z')$ between unit

charges at $(\mathbf{r},z)$ and $(\mathbf{r}',z')$ in the FET structure, $F(q)$ is related to the averaged 2D Fourier coefficient $V_F(q)=\langle V(q,z-z')\rangle_F$, where the average $\langle\ \rangle_F$ is taken over both z and z' coordinates and is implicitly defined by

$$V_F(q)=\frac{e^2}{q(\epsilon_{\mathrm{SiGe}}+\epsilon_{\mathrm{Si}})}F(q)\ .$$

$G(q,z)$ is related to the 2D Fourier coefficient of the averaged Coulomb potential $V_G(\mathbf{r},z)=\langle V(\mathbf{r},z-z')\rangle_G$, where the average $\langle\ \rangle_G$ is taken over the z' coordinate only and is defined by

$$V_G(q,z)=\frac{e^2}{q(\epsilon_{\mathrm{SiGe}}+\epsilon_{\mathrm{Si}})}G(q,z)\ .$$

Because of the envelope function (6), the 2D acoustic phonon scattering rate Γ_{ac} is given by[13]

$$\Gamma_{\mathrm{ac}}(k)=\frac{3b_0\Xi_a^2k_BTm_t}{16\hbar^3\rho s^2}\ , \tag{16}$$

where there is no explicit k dependence. Here Ξ_a is the effective deformation potential, ρ is the mechanical density, and s is the sound velocity, all of which are assumed to be the same as those of unstrained Si.[14] The scattering is reasonably regarded as being elastic and isotropic in the temperature range considered here. As discussed extensively in the literature, we assume that the effect of the interface on the phonon modes is irrelevant for low-field transport properties.[15,16]

The surface roughness scattering can be technologically reduced and does not provide a fundamental limit to the mobility, but is important in interpretation of an experimental result. The unscreened surface roughness scattering rate Γ_{SR} is given by[17]

$$\Gamma_{\mathrm{SR}}(k)=\frac{m_t\Delta^2L^2e^4n_s^2}{8\epsilon_{\mathrm{Si}}^2\hbar^3}\int_0^{2\pi}d\theta\exp(-q^2L^2/4)\ , \tag{17}$$

where again $q=2k\sin\theta/2$ is the momentum transfer in the scattering, Δ is the average displacement of the interface, and L is the correlation length of the roughness parallel to the interface. The integral in (17) can be written as a modified Bessel function, although the form (17) is more convenient for numerical calculation. The screening factor $[1+q_0F(q)\Pi(q)/q]^{-2}$ is not assumed in the integrand, unlike Ref. 12. The role of screening is difficult to ascertain from experiment, as the surface roughness parameters give two fitting constants. The approach here maximizes the effect of surface roughness scattering.

A Monte Carlo simulation has been performed using the above scattering models. Since we are interested in low-temperature and low-field transport, the usual method to study the response of the system to the applied electric field has a stability problem due to infrequent phonon scattering. We follow a different procedure for low fields,[18] and the diffusion constant D is evaluated from the mean-square displacement $\langle\Delta x(t)^2\rangle$ that is ensemble-averaged in the equilibrium simulation by[19]

$$D=\frac{1}{2}\frac{d\langle\Delta x(t)^2\rangle}{dt}\ . \tag{18}$$

This is converted to mobility μ with the help of the Einstein relation. The general form of the Einstein relation applicable even for 2D degenerate electrons is given by[17]

$$\mu=\frac{eD}{n_s}\frac{\partial n_s}{\partial E_F}\ , \tag{19}$$

where the 2D electron density n_s is given by (1). This relation reduces to $\mu=eD/E_{F0}$ for $E_{F0}\gg k_BT$ with $E_{F0}=E_F-E_0$, which is dominated by the behavior of the electrons near E_F, and $\mu=eD/k_BT$ for $-E_{F0}\gg k_BT$, which reflects the behavior of all the electrons.

The inclusion of Fermi-Dirac statistics in the Monte Carlo simulation is essential when $E_{F0}\gg k_BT$. Since all the scatterers considered here are elastic and the simulations are performed in a near thermal equilibrium condition (negligible electric field), each electron is assumed to not change its energy throughout the simulation. In this case, the effect of Fermi-Dirac statistics—only the electrons near the Fermi energy can participate in the transport—can be included in the evaluation of D by restricting the ensemble electrons to be near the Fermi surface. Instead of assigning an initial electron energy given by the energy distribution $f(E)$ and using a rejection technique in the scattering process[20] to incorporate the Pauli exclusion principle, we generate an initial energy E_i for each electron so that the effective energy distribution will be given by $f(E)[1-f(E)]$, where $f(E)$ is the temperature-dependent Fermi-Dirac function. The rejection technique is not necessary in the present method since the Pauli exclusion principle is included in the initial energy distribution of electrons. The initial electron energy is generated by using a random number r uniformly distributed over (0,1) by

$$E_i=k_BT\ln\left[\frac{1-r}{r}\exp(E_{F0}/k_BT)+\frac{1}{r}\right]\ . \tag{20}$$

It can easily be seen that the expression (20) yields a sharply peaked energy distribution $\delta(E-E_{F0})$ when $E_{F0}\gg k_BT$ and a Boltzmann distribution $\exp(-E/k_BT)$ when $-E_{F0}\gg k_BT$ (if multiplied by proper normalization constants).

III. RESULTS AND DISCUSSION

Figure 2 shows the velocity autocorrelation function and the mean-square displacement for a doped 2×10^{18} cm^{-3} $\mathrm{Si}_{0.7}\mathrm{Ge}_{0.3}$ layer with an undoped $\mathrm{Si}_{0.7}\mathrm{Ge}_{0.3}$ 10-nm spacer from the active Si channel at 4.2 K, assuming only the fundamental scattering mechanisms of acoustic phonon scattering and remote impurity scattering. It is clearly seen that the velocity autocorrelation function has a simple exponential dependence on time and the mean-square displacement is linearly dependent on time except for $t<30$ ps, where t is less than the relaxation time determined by impurity scattering and acoustic phonon scattering, and the transient has not settled out.[21] It is straightforward to evaluate the diffusion constant D by (18) and convert it to the mobility μ by (19), which gives $\mu=2.5\times10^5$ $\mathrm{cm}^2/\mathrm{V\,s}$.

Figure 3 shows the electron density and the mobility as

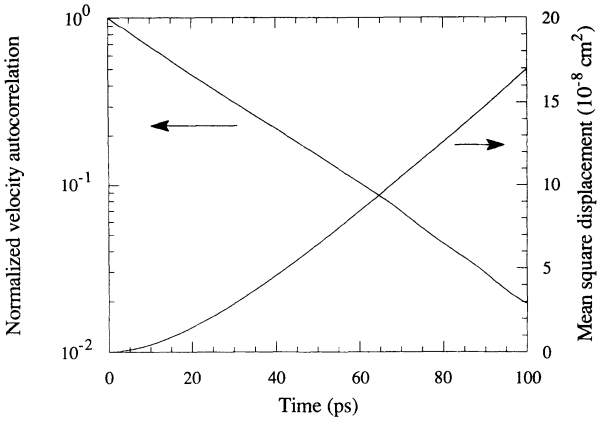

FIG. 2. Velocity autocorrelation function and mean-square displacement for a 2×10^{18} cm^{-3} doped $Si_{0.3}Ge_{0.7}$ layer with a 10-nm undoped $Si_{0.3}Ge_{0.7}$ spacer from the active Si channel at 4.2 K, assuming only the fundamental scattering mechanisms of acoustic phonon scattering and remote impurity scattering.

a function of the width of the undoped $Si_{0.7}Ge_{0.3}$ spacer at 4.2 and 1.5 K. The inclusion of the temperature-momentum-dependent polarizability function is essential for a quantitative discussion. The mobility reaches 2.5×10^5 cm^2/V s at 4.2 K and 3.1×10^5 cm^2/V s at 1.5 K for the width of 10 nm, and 5.0×10^5 and 7.6×10^5 cm^2/V s, respectively, for the width of 20 nm. The channel electron density shows practically no temperature dependence at these low temperatures and is 7.5×10^{11} cm^{-2} for the width of 10 nm and 4.6×10^{11} cm^{-2} for the width of 20 nm. When the spacer is thinner than 7.5 nm, the mobility at 4.2 K is larger than that at 1.5 K. This happens when the impurity scattering is so frequent that the resulting mobility is small: If we increase the characteristic electron energy participating in the transport by either raising the temperature or the Fermi energy (the former corresponds to the present case), the impurity scattering rate decreases due to the property of the Coulomb potential and the mobility increases.[10] The rapid increase in mobility with the spacer width indicates that the remote impurity scattering dominates electron transport in this modulation-doped structure at both temperatures. The product of the electron density and mobility increases monotonically with the spacer width, and this suggests that the use of a wider spacer is advantageous for some applications. As is remarked in Sec. II, the depleted width w of the doped $Si_{0.7}Ge_{0.3}$ is proportional to n_s by the relation due to the charge neutrality condition $w=n_s/N_{SiGe}$ and has the same functional dependence as n_s.

Figure 4 shows the electron density and mobility as a function of the doping concentration in the $Si_{0.7}Ge_{0.3}$ layer with a 10-nm undoped $Si_{0.7}Ge_{0.3}$ spacer at 4.2 and 1.5 K. The high-doping limit corresponds to δ doping,[22] which is advantageous in controlling the 2D electron density. Because of the dominant remote impurity scattering, the mobility decreases rapidly with the doping concentration. The product of the electron density and the mobility is monotonically decreasing with increasing doping concentration, since the reduction in mobility is more significant than the increase in electron density. Higher doping is advantageous in controlling the electron density, but may not increase the product due to the reduction of the mobility-density product. This trend is enhanced if surface roughness scattering, which is more frequent for higher electron densities $\Gamma_{SR}\sim n_s^2$ as shown in (17), is present.

Figure 5 shows the electron mobility as a function of temperature for a 2×10^{18} cm^{-3} doped $Si_{0.7}Ge_{0.3}$ layer with a 10-nm undoped $Si_{0.7}Ge_{0.3}$ spacer. For reference, the experimental result of Ref. 1 for the same doping concentration and the spacer width is plotted in the figure by empty squares. The calculated mobility, denoted as fundamental limit in the figure, monotonically decreases with the temperature in the present situation, and this is consistent with many reported experiments.[1,2] This is because the acoustic phonon scattering becomes more frequent with temperature as shown in (16) and tends to reduce mobility with increasing temperature, which we

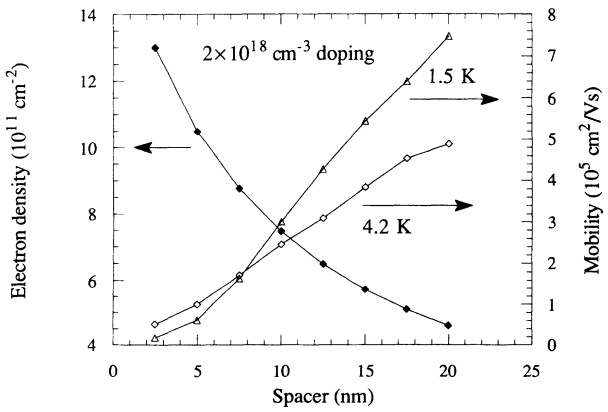

FIG. 3. Electron density and mobility as a function of spacer width for a 2×10^{18} cm^{-3} doped $Si_{0.7}Ge_{0.3}$ layer at 1.5 and 4.2 K with acoustic phonon and remote impurity scattering only.

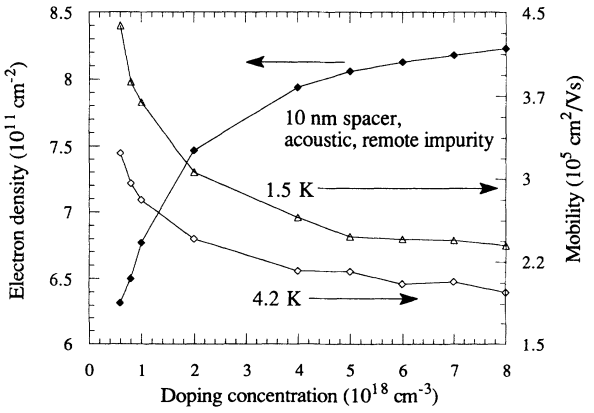

FIG. 4. Electron density and mobility as a function of the doping concentration in the $Si_{0.;7}Ge_{0.3}$ layer with a 10-nm undoped $Si_{0.7}Ge_{0.3}$ spacer at 1.5 and 4.2 K with acoustic phonon and remote impurity scattering only.

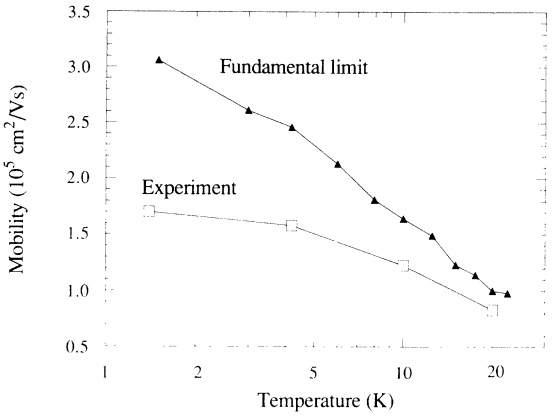

FIG. 5. Electron mobilty as a function of temperature for a 2×10^{18} cm^{-3} doped $Si_{0.7}Ge_{0.3}$ layer with a 10-nm undoped $Si_{0.7}Ge_{0.3}$ spacer with acoustic phonon and remote impurity scattering only. The calculated mobility is denoted as fundamental limit and the experimental result of Ref. 1 is shown by empty squares.

have observed here. The calculated mobility values are about a factor of 2 higher than the experimental ones, and this discrepancy can be attributed to the additional scattering mechanisms such as surface roughness scattering or interface/background impurity scattering.

Figure 6 summarizes this and shows the electron mobility as a function of temperature with one additional scattering. The experimental result of Ref. 1 can be recovered by assuming either one of the following scattering mechanisms is added to the fundamental mechanisms of remote impurity scattering and acoustic phonon scattering considered so far: (i) interface impurity scattering with a concentration of 10^{10} cm^{-2}, or (ii) background impurity scattering with the concentration of

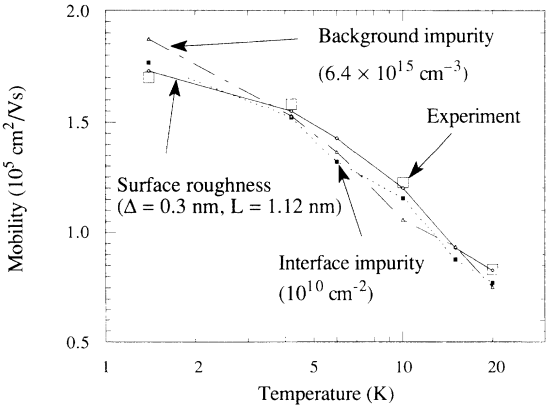

FIG. 6. Electron mobility with addition of surface roughness scattering, interface impurity scattering, or background impurity scattering. The experimental result of Ref. 1 is shown by empty squares. The solid line shows the result of additional surface roughness scattering ($\Delta=0.3$ nm and $L=1.12$ nm), the dashed line shows that of interface impurity scattering (10^{10} cm^{-2}), and the dash-dotted line shows that of background impurity scattering (6.4×10^{15} cm^{-3}).

6.4×10^{15} cm^{-3}, or (iii) surface roughness scattering with $\Delta=0.3$ nm and $L=1.12$ nm using the unscreened model. This combination of Δ and L is just one example out of many possibilities. In fact, the experimental result is also well recovered for $\Delta=0.34$ nm and $L=1$ nm. If the screened model including the image field effect in Ref. 12 is used for surface roughness scattering, then again there are many possibilities and some examples that can recover the experimental result are $\Delta=0.5$ nm and $L=14$ nm, or $\Delta=1$ nm and $L=22$ nm. We note that L is one order of magnitude larger than that of the unscreened model. In the treatment of interface/background impurity scattering, impurities are assumed to be compensated properly so that there is no effect for the channel electron density. If not compensated, they affect the electron density and the method to estimate the electron density developed in (1)–(5) in Sec. II has to be modified accordingly. As is clear in the figure, any of these scattering mechanisms can explain the experimental result very well. It is also quite possible that some of these mechanisms coexist and contribute to the mobility. At this stage, we cannot determine which is the most likely mechanism (or which is the most likely combination) to explain the discrepancy with the experimental result.

When transport at higher temperatures is considered, we need to include the raised valleys as well as higher subbands in the lowered valleys. This will change the physical picture of confined 2D electrons since the $Si_{0.7}Ge_{0.3}$ layer may not always be a potential barrier to the electrons if they are in the raised valleys,[5] and the 3D nature of electrons would emerge. The modification is also expected for the screening factor $G(q,z)^2[1+q_0F(q)\pi(q)/q]^{-2}$, through the change in the form factors $F(q)$ in (13) and $G(q,z)$ in (14), where the electron distribution function in the normal direction to the heterointerface is no longer a squared envelope function for the lowest subband. These are left for future work. It should be noted that the transport in the high-temperature limit can be modeled easily, since a 3D description of electrons would be a reasonable approximation.[6]

IV. CONCLUSION

A Monte Carlo simulation has been performed to study the electron mobility in the $Si/Si_{1-x}Ge_x$ system at low temperatures. The diffusion constant is evaluated in thermal equilibrium simulations and is converted to the mobility by use of the Einstein relation for a degenerate 2D electron gas. We consider a modulation-doped structure, where the doped $Si_{0.7}Si_{0.3}$ layer is separated by a $Si_{0.7}Ge_{0.3}$ spacer layer, and the electron density is evaluated as a function of spacer width and doping concentration. Electrons are assumed only in the lowest subband. We have found peak mobility values of 2.5×10^5 cm^2/V s at 4.2 K and 3.1×10^5 cm^2/V s at 1.5 K, limited by acoustic phonon and impurity scattering at an electron density of 7.5×10^{11} cm^{-2}, for a 10-nm spacer and 2×10^{18} cm^{-3} doping. Mobility values 5.0×10^5 cm^2/V s at 4.2 K and 7.6×10^5 cm^2/V s at 1.5 K are achieved for larger spacer layers (with corresponding lower channel electron densi-

ties). The effect of surface roughness scattering as well as other impurity scattering has also been discussed, which can explain the difference between the peak mobility values found here and the reported experimental data.

ACKNOWLEDGMENT

This work was supported in part by the Office of Naval Research.

*On leave from Fujitsu Basic Process Development Division, Kawasaki, Japan.

[1]D. Többen, F. Schäffler, A. Zrenner, and G. Abstreiter, Phys. Rev. B **46**, 4344 (1992).

[2]Y. J. Mii, Y.-H. Xie, E. A. Fitzgerald, D. Monroe, F. A. Thiel, and E. B. Weir, Appl. Phys. Lett. **59**, 1611 (1991).

[3]D. Monroe, Y.-H. Xie, E. A. Fitzgerald, P. J. Silverman, and G. P. Watson, J. Vac. Sci. Technol. B **11**, 1731 (1993).

[4]K. Ismail, B. S. Meyerson, S. Rishton, J. Chu, S. Nelson, and J. Nocera, IEEE Trans. Electron Device Lett. **13**, 229 (1992).

[5]G. Abstreiter, H. Brugger, T. Wolf, H. Jorke, and H. J. Herog, Phys. Rev. Lett. **54**, 2441 (1985); R. People, IEEE J. Quantum Electron. **22**, 1696 (1985).

[6]H. Miyata, T. Yamada, and D. K. Ferry, Appl. Phys. Lett. **62**, 2661 (1993).

[7]F. F. Fang and W. E. Howard, Phys. Rev. Lett. **16**, 797 (1966); F. Stern, Phys. Rev. B **5**, 4891 (1972).

[8]D. Delagebeaudeuf and N. T. Linh, IEEE Trans. Electron Devices **29**, 955 (1982).

[9]P. F. Maldague, Surf. Sci. **73**, 296 (1978); F. Stern, Phys. Rev. Lett. **44**, 1469 (1980).

[10]F. Stern and S. E. Laux, Appl. Phys. Lett. **61**, 1110 (1992).

[11]F. Stern and W. E. Howard, Phys. Rev. **163**, 816 (1967).

[12]T. Ando, A. B. Fowler, and F. Stern, Rev. Mod. Phys. **54**, 437 (1982).

[13]P. J. Price, Ann. Phys. (N.Y.) **133**, 217 (1981).

[14]M. M. Rieger, Diplom thesis, Technical University Munich, 1991.

[15]P. Lugli, P. Bordone, S. Gualdi, P. Poli, and S. M. Goodnick, Solid State Electron. **32**, 1881 (1989), and references therein.

[16]B. T. Moore and D. K. Ferry, J. Vac. Sci. Technol. **17**, 1037 (1980).

[17]D. K. Ferry, *Semiconductors* (Macmillan, New York, 1991).

[18]M. A. Littlejohn, J. R. Hauser, and T. Glisson, Appl. Phys. Lett. **26**, 625 (1975).

[19]T. Yamada and D. K. Ferry, Phys. Rev. B **47**, 1444 (1993); **47**, 6416 (1993).

[20]P. Lugli and D. K. Ferry, IEEE Trans. Electron Devices **32**, 2431 (1985); S. Bosi and C. Jacoboni, J. Phys. C **9**, 315 (1976).

[21]R. Kubo, in *Transport Phenomena,* edited by G. Kirkaenow and J. Marro, Lecture Notes in Physics Vol. 31 (Springer-Verlag, Berlin, 1974).

[22]H.-J. Gossmann, E. F. Schubert, D. J. Eaglesham, and M. Cerullo, Appl. Phys. Lett. **57**, 2440 (1990).